ELSEVIER

International Journal of Heat and Fluid Flow 23 (2002) 161–172

International Journal of HEAT AND FLUID FLOW

www.elsevier.com/locate/ijhff

Scalar dispersion from an instantaneous line source at the wall of a turbulent channel for medium and high Prandtl number fluids

Dimitrios V. Papavassiliou *

School of Chemical Engineering and Materials Science, The University of Oklahoma, 100 East Boyd Street, SEC T-335, Norman, OK 73019, USA

Abstract

Lagrangian methods have been used recently to reconstruct temperature profiles for relatively high Prandtl number, Pr, fluids (up to $Pr = 2400$) in direct numerical simulations (DNS) of turbulent channel flow. The basic concept is that a heated surface is formed by an infinite number of continuous sources of heat. For example, the behavior of a heated plane can be synthesized by the behavior of an infinite number of continuous sources of heat that cover the plane. The building block for such a reconstruction is the behavior of a single instantaneous heat source located at the wall. The present work studies the behavior of such sources in turbulent channel flow. The trajectories of heat markers are monitored in space and time as they move in a hydrodynamic field created by a DNS. The fluids span several orders of magnitude of Pr (or Sc), $Pr = 0.1$, 1, 10, 100, 200, 500, 2400, 7000, 15 000, 50 000, (liquid metals, gases, liquids, lubricants and electrochemical fluids). The effects of Pr in the evolution of the marker cloud are examined and quantified. The marker cloud is found to evolve in three stages, two of which are Pr dependent.

Keywords: Lagrangian tracking; Direct numerical simulation; Prandtl number; Source diffusion

1. Introduction

A basic problem in developing a theory for turbulent transport of mass or heat from a wall is to calculate statistical properties of the scalar field from statistical properties of the velocity field. Central concerns are the prediction of the spatial variation of eddy transport coefficients, the effect of molecular Prandtl number, Pr, on turbulent transport and the effect of boundary condition changes on the transport properties. The classical approach has been to use some form of the Reynolds analogy to relate turbulent transport of a scalar to turbulent transport of momentum (the Reynolds stress). Even though the use of averaged equations or models based on the analogy is standard engineering practice, it might lead to inaccuracies (Churchill, 1996, 1997).

Direct numerical simulations (DNS) of turbulent flows and of scalar turbulent transport offer the opportunity to address such issues and to provide a sounder theoretical understanding than is offered by the analogy. These simulations are based on first principles and they are equivalent to extremely accurate experiments (Moin and Mahesh, 1998; Kasagi and Shikazono, 1995). Computational requirements, however, have limited DNS applications to a narrow range of fluids with molecular Pr or Schmidt number, Sc, between 0.025 and 10 (Kim and Moin, 1989; Lyons et al., 1991a; Kasagi et al., 1992; Kasagi and Shikazono, 1995; Kawamura et al., 1998; Kawamura et al., 1999; Na et al., 1999; Na and Hanratty, 2000; Tiselj et al., 2001). This limitation arises because, in order to resolve all the scales of motion and temperature, the number of grid points has to be analogous to $Pr^{3/2}Re^{9/4}$. An increase of Pr by one order of magnitude means an increase of the number of grid points by about 30 times. In addition, each simulation describes a specific configuration (isothermal walls or constant heat flux walls). Calmet and Magnaudet (1997) used Large Eddy Simulation to study turbulent mass transfer for Sc in the range $1 \leqslant Sc \leqslant 200$. Using Lagrangian methods, Papavassiliou and Hanratty (1997) reconstructed temperature profiles for higher Pr by orders of magnitude (up to $Pr = 2400$) and different problem configurations without increasing the number of grid points. The behavior of a heated plane was synthesized by the behavior of an infinite number of continuous sources of heat that covered the

* Tel.: +1-405-325-5811; fax: +1-405-325-5813.
E-mail address: dvpapava@ou.edu (D.V. Papavassiliou).

0142-727X/02/$ - see front matter
PII: S0142-727X(01)00146-1

Nomenclature

b	Batchelor's constant
D	molecular diffusivity
h	half channel height
P_1	probability density function for a puff of heat
P_2	probability density function for a plume of heat
Pr	Prandtl number, $Pr = \nu/\alpha$
R^{L}	Lagrangian correlation coefficient
$R_{V_iV_j}$	material correlation coefficient for marker velocities
$R_{V_i^m V_j^m}$	material correlation coefficient for marker–marker velocities
Re	Reynolds number
Sc	Schmidt number, $Sc = \nu/D$
T	temperature
t	time
$\underline{X}(\underline{x}_0, t)$	position vector at time t for a marker released at $\underline{x}_0$
X, Y, Z	marker position in respective direction
x, y, z	streamwise, normal and spanwise coordinates
$\underline{x}_0$	marker position at time zero
$\underline{U}$	Eulerian velocity vector
u, v, w	streamwise, normal and spanwise velocities
u^*	friction velocity
$\underline{V}$	Lagrangian velocity vector of a marker
$\overline{\underline{V}}$	mean marker cloud velocity

Greeks

α	thermal diffusivity
Δt	time step
ν	kinematic viscosity of the fluid
σ	standard deviation of the random molecular jump of heat markers
τ	time
τ_i^{L}	Lagrangian timescale in the i-direction
τ_{95}	timescale for 95% dispersion due to molecular diffusion effects
$\tau_{\text{zone II}}$, $\tau_{\text{zone III}}$	timescale characteristic of the stages of puff development

Superscripts

$()'$	fluctuations
$()^+$	quantity in viscous wall units

plate (Papavassiliou and Hanratty, 1995). This technique, which we will refer to as the Lagrangian scalar tracking (LST) method, has also been implemented successfully by Ponoth and McLaughlin (2000) for the simulation of mass transfer in low Re fluids and non-Cartesian geometries for bubble dissolution in the presence of surfactants.

In the Lagrangian framework, contrary to the Eulerian framework, the system of reference moves with the fluid particles, or the heat or mass markers in the case of scalar transport. The Lagrangian approach is the natural mechanism of transport and it can provide valuable physical insights. Another advantage of LST is that a single computation can be used to reconstruct the behavior in different problem configurations; e.g., isothermal and isoflux walls, step change in wall temperature or heat flux, continuous and instantaneous line source behavior.

The building block for such a reconstruction is the behavior of a scalar line source located at the wall. The present work studies the behavior of such sources in turbulent channel flow. A tracking algorithm is used to monitor the trajectories of particles in space and time as they move in a hydrodynamic field created by a DNS. The fluids span several orders of magnitude of Pr (or Sc), $Pr = 0.1$, 1, 10, 100, 200, 500, 2400, 7000, 15 000, 50 000, (liquid metals, gases, liquids, lubricants and electrochemical fluids). The focus of this paper is the description of the behavior of an instantaneous line source with an emphasis on the higher Pr fluids.

2. Background

Einstein (1905) developed a relation that describes dispersion of particles in terms of the mean-squared displacement from the source in the x-direction:

$$\mathrm{d}\overline{X^2}/\mathrm{d}t = 2D, \tag{1}$$

where D is the molecular diffusivity. Taylor (1921) developed a similar relation for the rate of dispersion of fluid particles from a point source in homogeneous, isotropic turbulence:

$$\frac{\mathrm{d}\overline{X^2}}{\mathrm{d}t} = 2\overline{u^2}\int_0^t R^{\mathrm{L}}(\tau)\,\mathrm{d}\tau, \tag{2}$$

where $\overline{u^2}$ is the mean-square of the x-component of the velocity of fluid particles and R^{L} is the Lagrangian correlation coefficient. An important implication of Taylor's equation is that the history of the particle motion affects the rate of dispersion through R^{L}. At small times, the value of the Lagrangian correlation coefficient is close to one, and the dispersion increases with time to the second power. At large times it is $R^{\mathrm{L}} = 0$, and the dispersion changes linearly with time.

Dispersion of heat or mass markers introduces an additional complication, since the markers can move off a fluid particle as a result of molecular diffusion. Saffman (1960) developed a relation for dispersion in this case by defining a material autocorrelation function, which correlates fluid velocity components along the trajectories of markers instead of fluid particles. Corrsin

(1953, 1959) studied line source diffusion in a homogeneous shear flow with a constant mean velocity gradient. The Lagrangian dispersion in the direction of the flow, X, was found to be different from the dispersion in the direction of the velocity gradient, Y, which is described by Taylor's analysis. It is

$$Y = \int_0^t v(t_1)\,\mathrm{d}t_1 \tag{3a}$$

and

$$X = \int_0^t \left[\frac{\mathrm{d}\overline{U}}{\mathrm{d}y}Y(t_1) + u(t_1)\right]\mathrm{d}t_1, \tag{3b}$$

where u, v are the particle velocities in the direction of the flow and in the direction of the velocity gradient, respectively. For large times the dispersion becomes (Corrsin, 1959)

$$\overline{Y^2} = 2\overline{v^2}\tau_y^{\mathrm{L}}t \tag{4a}$$

and

$$\overline{X^2} = \frac{2}{3}\left(\frac{\mathrm{d}\overline{U}}{\mathrm{d}y}\right)^2\overline{v^2}\tau_y^{\mathrm{L}}t^3, \tag{4b}$$

where τ_y^{L} is the Lagrangian timescale in the y-direction.

Hanratty (1956) used Taylor's theory to describe the transfer of heat in a homogeneous isotropic flow between a hot and a cold wall. An infinite number of line sources of heat along one wall was used to describe the hot plane and an infinite number of line sinks of heat along the other wall described the behavior of the cold plane.

The Lagrangian approach has been used to interpret observations in the Eulerian framework with fundamental arguments: (a) the variation of the eddy conductivity with the distance from the wall has been associated with the time dependency of turbulent diffusion, specifically the time that the heat markers have been in the flow field (Eckelman and Hanratty, 1972), and (b) temperature gradients close to the wall are the result of the behavior of thermal markers that have been in the field for small periods of time.

The behavior of individual point and line sources in the turbulent field is needed to apply Hanratty's Lagrangian approach. Batchelor (1964) developed a theory for the prediction of the statistical behavior of a source in a turbulent boundary layer. He used similarity to argue that the Lagrangian velocity within the constant stress region depends only on the friction velocity u^* and time so that

$$\overline{V_y} \equiv \frac{\mathrm{d}\overline{Y}}{\mathrm{d}t} = bu^*, \tag{5}$$

where b is an absolute constant. Batchelor estimated the value of b to be 0.2 (based on experimental results by Townsend) and Shlien and Corrsin (1976) measured $b = 0.39$ for the case of $Pr = 0.7$.

Laboratory measurements for turbulent dispersion have been reported for the case of continuous sources of a passive scalar (Poreh and Cermak, 1964; Shlien and Corrsin, 1976; Fackrell and Robins, 1982; Raupach and Legg, 1983; Incropera et al., 1986). However, none of these provide space–time correlations for the behavior of single instantaneous sources. Poreh and Cermak (1964) measured the dispersion of ammonia gas from a continuous line source located at the wall of a turbulent boundary layer. They distinguished four zones of dispersion: (a) the initial zone, in which almost all the contaminant is near the wall; (b) the intermediate zone, in which a plume is diffusing submerged in the boundary layer; (c) the transition zone, in which the edge of the turbulent boundary layer behaves as a "lid" and allows dispersion through it only with molecular diffusion; and (d) the final zone, in which all the contaminant is contained between the wall and the edge of the boundary layer. Shlien and Corrsin (1976) examined turbulent dispersion of heat in a wind tunnel, downstream from a heated wire. Qualitative interpretation of their results confirmed the four stages observed with the mass transfer results of Poreh and Cermak and showed good quantitative agreement, specifically in the intermediate stage.

3. Methodology

The present work is focused on the Lagrangian behavior of sources in an inhomogeneous turbulent field. The velocity field for a Newtonian and incompressible fluid is calculated using a DNS of fully developed turbulent flow in a channel, which was developed by Lyons et al. (1991b). The Reynolds number, Re, defined with the centerline mean velocity and half-height of the channel, h, is 2660. The simulation is done on a $128 \times 65 \times 128$ grid in (x, y, z). The dimensions of the computational box are $(4\pi h, 2h, 2\pi h)$, with $h = 150$ in wall units. The flow is assumed to be periodic in the streamwise and spanwise directions with periodicity lengths equal to the dimensions of the box in the respective directions.

A tracking algorithm (Kontomaris et al., 1993) is used to monitor the trajectories of particles in space and time as they move in the hydrodynamic field created by the DNS. The basic assumption is that a heat marker at each time has the velocity of the fluid particle that carries it, $\underline{V}(\underline{x}_0, t) = \underline{U}[\underline{X}(\underline{x}_0, t), t]$, where $\underline{V}(\underline{x}_0, t)$ is the Lagrangian velocity of a marker that is released at location $\underline{x}_0$ and $\underline{U}$ is the Eulerian velocity. The equation of particle motion then is

$$\underline{V}(\underline{x}_0, t) = \frac{\partial \underline{X}(\underline{x}_0, t)}{\partial t}. \tag{6}$$

The motion of the heat markers is decomposed into a convection part and a molecular diffusion part. The

convective part can be calculated from the fluid velocity at the particle position (using Eq. 6 and the velocity from the DNS). The effect of molecular diffusion follows from Einstein's theory for Brownian motion. It is simulated by imposing a 3D random walk on the particle motion, which is added on to the convective part of the motion after each time step, Δt, and it takes values from a Gaussian distribution with zero mean and standard deviation $\sigma = \sqrt{2\Delta t D}$. Using viscous wall units, the standard deviation becomes $\sigma^+ = \sqrt{2\Delta t^+/Pr}$. This is the mechanism that incorporates the effect of the fluid Sc or Pr in the numerical process. The time step for the calculations of the hydrodynamic field and the Lagrangian tracking was $\Delta t^+ = 0.25$ in wall units. The choice of this time step for the Lagrangian calculations ensured that a marker has a very small probability to jump more than one hydrodynamic grid cell in one time step, $\sigma^+ < \Delta y^+$, in all Pr considered in this work. It is our experience that a smaller time step has to be used at the initial stages of marker release when working with Pr smaller than 0.1. Note that the limitations on Pr that restrict Eulerian simulations, as discussed in the introduction, do not restrict LST. The presence of these markers does not affect the flow field, so the behavior of a passive scalar is simulated.

4. Results

A total of 16 129 markers were released instantaneously from a uniform rectangular grid that covered the bottom wall of the channel in each of three runs. Run A tracked markers with $Pr = 0.1$, 1, 10 and 100 up to time $t^+ = 2750$, run B tracked markers with $Pr = 0.7$, 1, 3, 500 and 2400 up to time $t^+ = 2750$, and run C tracked markers with $Pr = 200$, 2400, 7000, 15 000 and 50 000 up to time $t^+ = 13\,000$.

The initial positions of the markers were on a 127×127 grid, so that a single marker was released from the middle of each edge of the hydrodynamic grid. The choice to release markers at one grid spacing apart was made in order to avoid the release of several markers from points in the flow that are strongly correlated. Calculations of the mean cloud position and of the root mean square of the marker positions around the mean using only every other marker (8065 total markers) have shown a difference of less than 2% in every case. Recent runs conducted in our laboratory (to be presented elsewhere), with one order of magnitude more markers in the flow, have shown a similar behavior. In general, the best criterion for determining whether enough markers have been used would be to calculate the statistical behavior of the cloud using a portion of them and then compare the results with the case of the total number of markers.

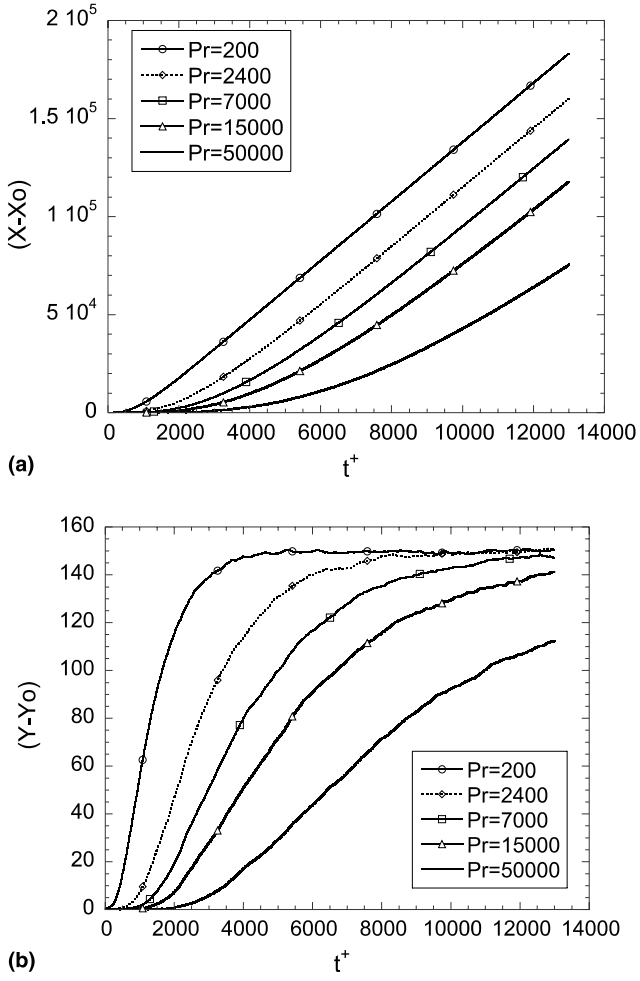

Fig. 1. Mean marker position for high Pr fluids (run C): (a) streamwise direction; (b) vertical direction.

Fig. 1 presents the mean trajectories, $\underline{X}(\underline{x}_0, t) - \underline{x}_0$, of the marker cloud of run C with time in the streamwise and normal directions. Physically, this is the trajectory of the centroid of a cloud of markers released from an instantaneous line source located at the wall of the channel. At large times, it is expected that the cloud will be uniformly distributed over the width of the channel and the centroid will be at $y = h = 150$. Lower Pr markers get away from the viscous wall region and into the region of higher mean velocity sooner than high Pr markers, because they move out of the wall region due to larger molecular jumps. Therefore, they advance much farther in the streamwise direction, as seen in Fig. 1(a). This indicates that entry effects in a channel with higher Pr fluid are felt for a much longer time. The density of the cloud of the markers is represented by the probability, $P_1(x, y, z, t|t_0, \underline{x}_0)$, of a marker to be at a location (x, y, z) in the flow field at time t, given that it was released at location $\underline{x}_0$ at time t_0. Fig. 2 presents the standard deviation of the probability of the marker

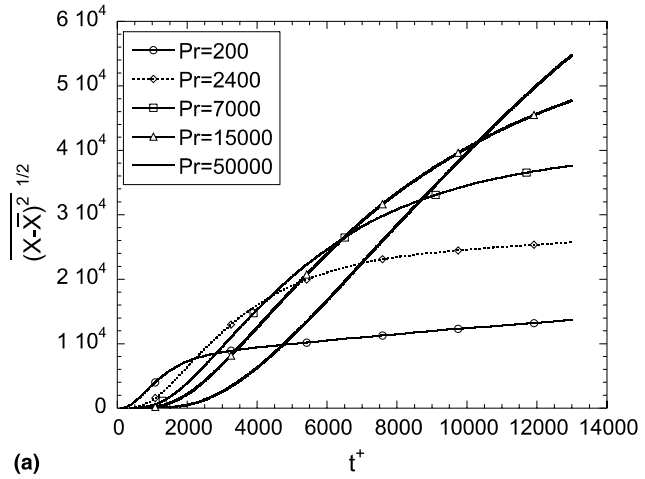

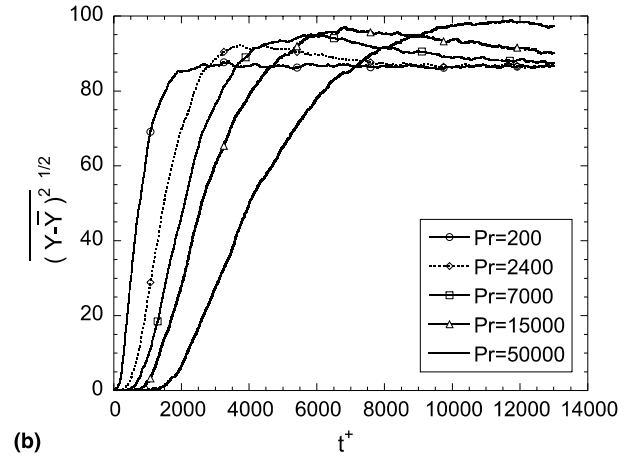

Fig. 2. Root mean square of the marker position relative to the cloud centroid for high *Pr* fluids (run C): (a) streamwise direction; (b) vertical direction.

location with time in the streamwise and the normal directions. In the streamwise direction, the standard deviation increases with *Pr*. As the *Pr* increases, a larger percentage of markers stay close to the wall for longer times. The markers that get in the outer region of the flow travel downstream with velocities close to the mean flow velocity. The conceptual picture that emerges for high *Pr* sources is that the front of the cloud moves with the mean flow velocity, while the back of the cloud stays in the viscous wall layer resulting: (a) in a cloud that is stretched downstream, and (b) in a high variance of the marker position in the streamwise direction. The standard deviation of the cloud position in the normal direction is expected to be that for a uniform distribution that extends throughout the width of the channel. This prediction is confirmed with the measurements presented in Fig. 2(b), where the normal direction standard deviation is shown to tend to the value of $(300^2/12)^{1/2} = 86.6$ at large times. A difference from this value, as seen for $Pr = 50000$, is an indication that the cloud has not developed to the point of uniformly covering the width of the channel.

The mean cloud velocities in the streamwise and in the normal directions are shown in Figs. 3(a) and (b), respectively. The streamwise velocity reaches the value of the bulk mean velocity of the flow field (close to 15 in wall units), as expected. The normal velocity of the cloud exhibits a maximum, as the cloud moves away from the wall on average, and then returns to zero, as the cloud covers the channel width uniformly.

The value of the constant *b* introduced by Batchelor (1964) is presented in Fig. 4 as a function of the *Pr*. The value was estimated using Eq. (5) at the maximum value of the normal Lagrangian velocity. After that point, the wall of the channel opposite to the source wall affects the evolution of the marker cloud. As presented in Fig. 4, the value of *b* is a function of *Pr*:

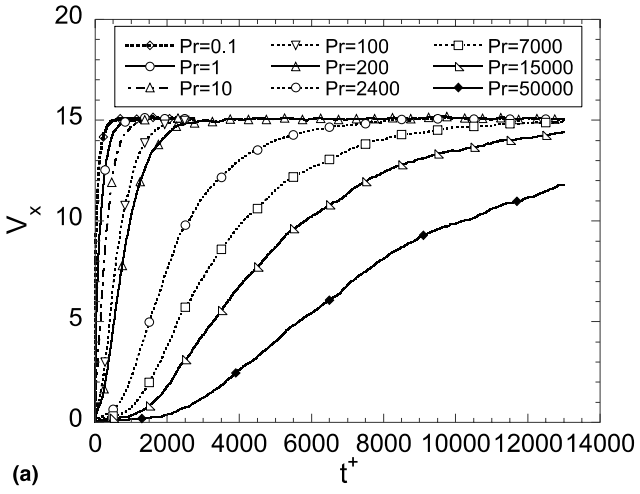

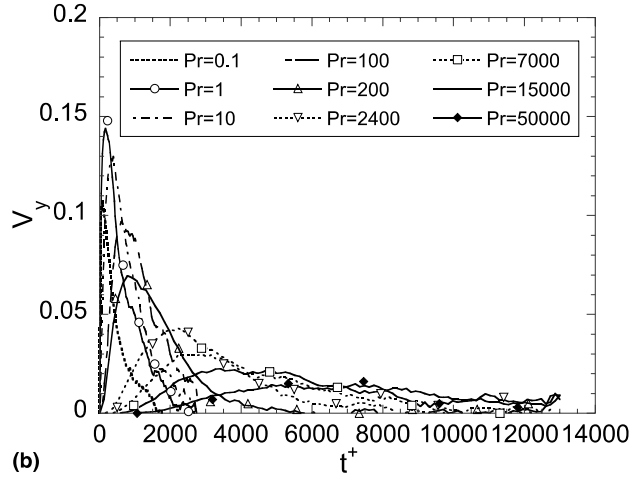

Fig. 3. Mean marker velocity for different *Pr* fluids: (a) streamwise direction; (b) vertical direction.

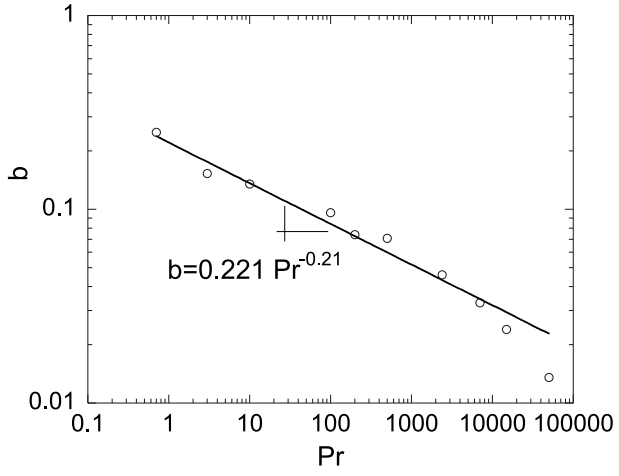

Fig. 4. Batchelor's constant as a function of the fluid *Pr*.

$$b = 0.221 Pr^{-0.21}. \quad (7)$$

At very high *Pr* the value of *b* goes to zero ($Pr \to \infty$ is the case of fluid particles, for which the Lagrangian normal velocity goes to zero), and at $Pr = 0.7$ (air at room temperature) the value of *b* goes to 0.238, which is close to the value of 0.2 predicted by Batchelor. Fig. 4 shows that the correlation expressed in Eq. (7) appears to work better for points with $Pr < 10\,000$. The physical reason is that, when the normal Lagrangian velocity of the cloud reaches its maximum, the mean cloud position is below the logarithmic region for the Eulerian velocity field. The similarity that applies in this case is the similarity of the viscous wall sublayer, not the similarity of the constant stress region, which applies to the cases of the lower *Pr*. In general, the channel flow configuration, which is employed in our numerical experiments, does not provide for an extended constant stress region. However, the dependence of Batchelor's constant on *Pr* is evident.

Fig. 5 shows the standard deviation of the probability of the markers that describes the streamwise and normal velocity, $\overline{(V_i - \overline{V}_i)^2}^{1/2}$, for runs A and C. There is a maximum for the streamwise velocity, which corresponds to the instant at which a cloud is exposed to drastically different mean velocities (a large part of it in the viscous layer with low mean velocity, and a part of it in the outer region with high mean velocity), and then a constant value, which corresponds to the final stage at which the cloud is uniformly distributed in the channel. At large times, it is expected that the standard deviation of the Lagrangian normal velocity will tend to the value of the average turbulent intensity of the Eulerian normal velocity across the channel. A similar observation for the streamwise velocity, however, should not be expected. In fact, the values for the streamwise velocity at large times are higher than the average across the

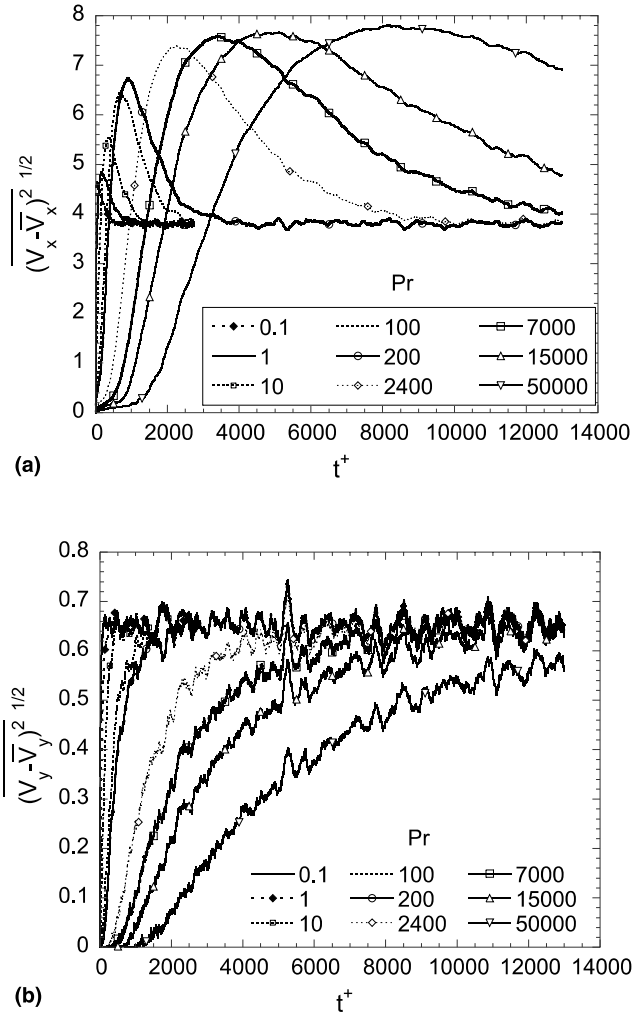

Fig. 5. Root mean square of the marker velocity relative to the cloud centroid for different *Pr* fluids: (a) streamwise direction; (b) vertical direction.

channel of the Eulerian streamwise turbulent intensity. This is because the Lagrangian velocity fluctuations are calculated with respect to the mean Lagrangian velocity of the cloud, which is the Eulerian bulk velocity of the fluid in the streamwise direction, and not relative to the ensemble average velocity of the flow field, as are the Eulerian velocity fluctuations. Fig. 5(b) also shows that after some time the standard deviation of the normal velocity for all *Pr* clouds for run A or run C follow similar patterns (recall that all cases for run A follow the same hydrodynamic field and all cases for run C follow another hydrodynamic field). This observation indicates that convection dominates transport when the markers leave the wall region independent of the *Pr*. Considering the fact that Eulerian mean temperature profiles for the case of a heated wall result from the behavior of an infinite number of wall sources, it appears that the differences between these profiles for different *Pr* are the

result of the fact that higher Pr markers stay longer in the viscous wall region. However, as soon as the markers arrive in the outer region, all Pr fluids behave in a similar way and turbulence mixes the markers well.

The cloud that results from an instantaneous source of a scalar is usually called a *puff* and the cloud that results from a continuous source of a scalar is usually called a *plume*. Fig. 6 presents contours of the probability density function P_1 for $Pr = 100$ markers at different times. The physical interpretation of these contours is that they represent temperature or concentration contours resulting from a puff released from a source instantaneously (Saffman, 1960). In this particular case of $Pr = 100$, three zones are observed that are reminiscent of the zones described by Poreh and Cermak (1964) for the case of plumes. Zone I, which corresponds to small times (see Fig. 6(a)), is characterized by the cloud staying together in a rather compact form close to the wall. In the second zone (zone II, shown in Figs. 6(b) and (c)), markers are leaking out of the compact cloud and into the outer region of the flow field where they get swept by the larger turbulence eddies and move with the mean flow velocity. The total cloud seems to be separated in two parts, the dissolving cloud in the viscous wall region and the markers that have leaked out of it and are forming a second group downstream from the

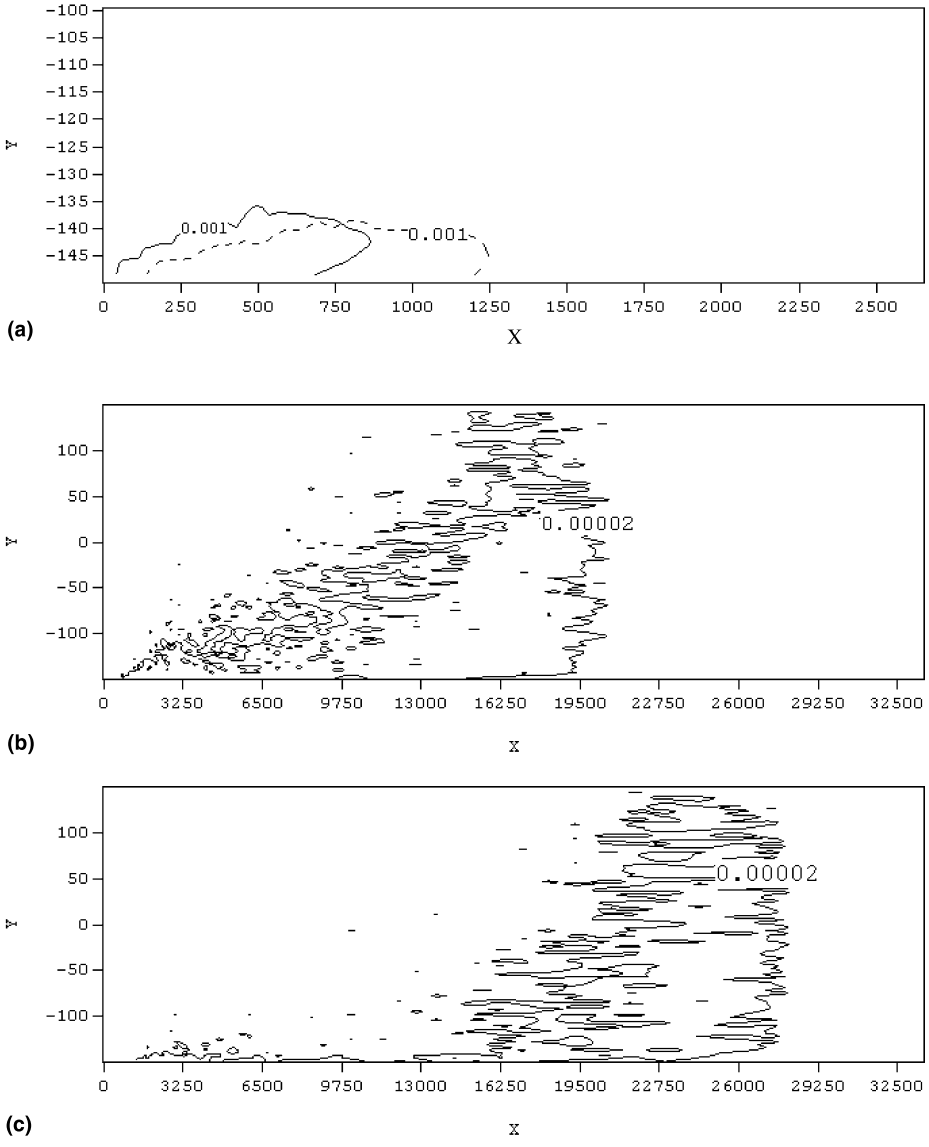

Fig. 6. Snapshots of a puff of markers with $Pr = 100$ at different times from their release: (a) $t^+ = 250$ and $t^+ = 500$; (b) $t^+ = 1500$; (c) $t^+ = 2000$. The bottom wall of the channel is at $y = -150$ and the top wall at $y = 150$.

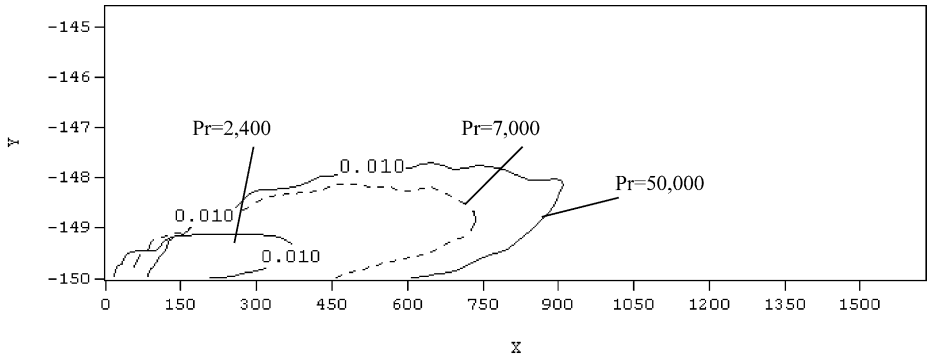

Fig. 7. Snapshots of a puff of markers at $t^+ = 1500$ from their release with different Pr: $Pr = 2400$, $Pr = 7000$, and $Pr = 50\,000$. The bottom wall of the channel is at $y = -150$ and the top wall at $y = 150$.

original cloud. In the third and final zone (zone III) the original tight cloud is dissolved into the outer flow. Our results show that this distinction in three zones is typical in the evolution of the puffs, especially for Pr larger than one. Contours of the puffs at other Pr (not presented here) show that zone II becomes more pronounced as Pr increases. The existence of this zone means that the information given by the mean particle position does not provide a complete picture for the puffs. The simple picture that the markers always form a cloud that is denser in its middle is not true for zone II. The cloud mean position is in fact located in a low concentration region between the two denser regions formed by the original cloud and the markers that have leaked out of it. This observation also indicates that the markers that reach the center of the channel in the case of plumes are not necessarily the ones that have been in the flow for a long time. At high Pr, it is quite possible that a particle that has been in the flow field for a long time stays in the wall region. There seems to be a filtering effect that allows fewer particles to leak away from the original puff as Pr increases. This observation is consistent with previous observations (Campbell and Hanratty, 1983; Hanratty and Vassiliadou, 1988; Calmet and Magnaudet, 1997) that different parts of the frequency spectrum of the velocity component normal to the wall, v, control turbulent transfer at different Pr. Experimental and numerical work in these papers showed that, as Pr increases, the frequencies of v fluctuations that contribute to turbulent transport from the wall decrease. The Lagrangian interpretation of the filtering effect, that the wall has on the turbulent structures contributing to transport, is that for higher Pr zone I is more extended. As Pr increases, the cloud of markers stays very close to the wall and only large eddy structures that reach into the viscous wall region from outside (those with low frequencies) can take markers away and can contribute to the leaking process that is characteristic of zone II.

Fig. 7 shows contours of the puff concentration at the same time ($t^+ = 1000$) and different Pr. The $Pr = 2400$ cloud is in zone II of development, while the higher Pr clouds are still in zone I. Fig. 7 shows that high Pr markers stay close to the wall for a long time. This fact can provide a physical interpretation in a Lagrangian

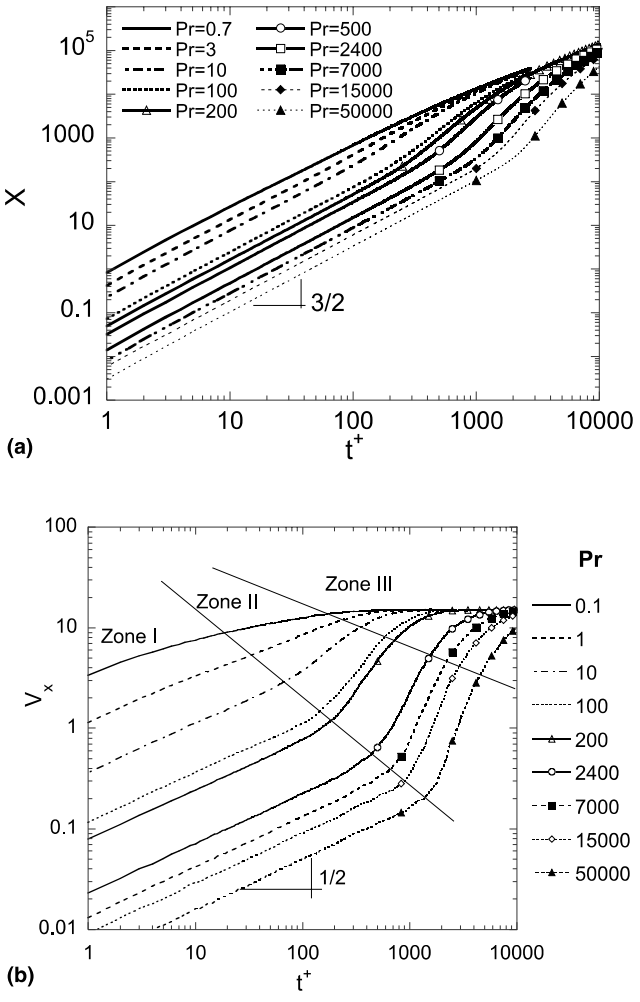

Fig. 8. Logarithmic plot of: (a) the streamwise cloud position; (b) the streamwise velocity.

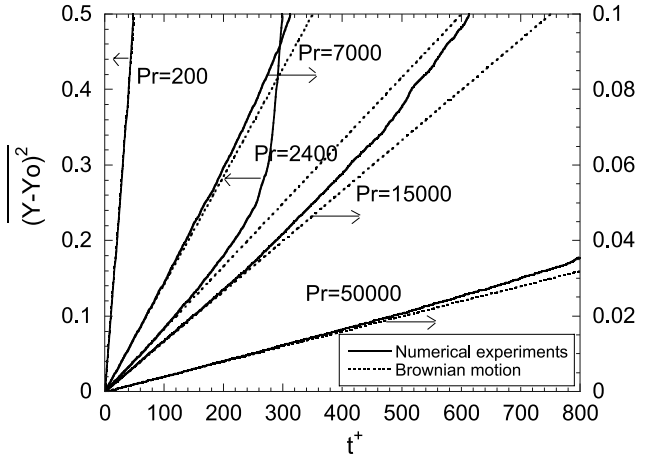

Fig. 9. Comparison of the dispersion of the cloud at the very early stages of cloud development to the dispersion by Brownian motion calculated by Einstein's relation.

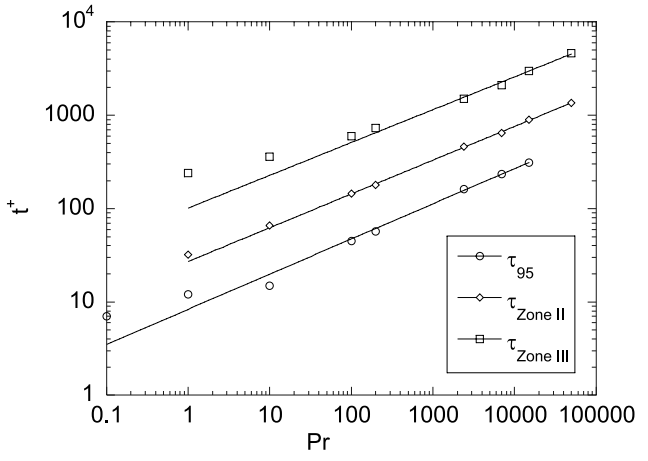

Fig. 10. Characteristic times for the evolution of a puff as a function of *Pr*.

sense for the shape of the mean temperature profile in the case of heat transfer from a wall. The Eulerian mean temperature presents a steep gradient close to the wall and then becomes flat away from the wall. The higher the *Pr*, the steeper the gradient and the flatter the outer region. The Eulerian interpretation is that turbulence has a better chance of mixing the high *Pr* fluids in the outer region, since the molecular diffusion is smaller. Keeping in mind that the mean temperature is affected by markers that were released from the wall at different times, it becomes now apparent that the reason for this behavior is the difficulty that the markers face to leave the viscous wall region and not the ability of turbulence to mix. As the *Pr* increases, the markers stay close to the wall resulting in steep temperature gradients. Relatively few get to the outer region resulting in flat temperature profiles.

Fig. 8 presents the mean cloud position and the mean cloud velocity as a function of time in logarithmic coordinates. The existence of the three zones of cloud development is presented in a clearer way than the qualitative observations in Fig. 6. Zone I, which is dominated by transfer with molecular means, is characterized by the relations: $X \propto t^{3/2}$ and $V_x \propto t^{1/2}$. The transition zone, zone II, is also a logarithmic zone that is more extended as *Pr* increases. The final zone, in which the dominant transport mechanism is turbulent convection, is shown as zone III.

The initial stage of cloud development, zone I, can be further split in two sub-regimes. The first sub-regime is identified as the zone that Brownian motion is the

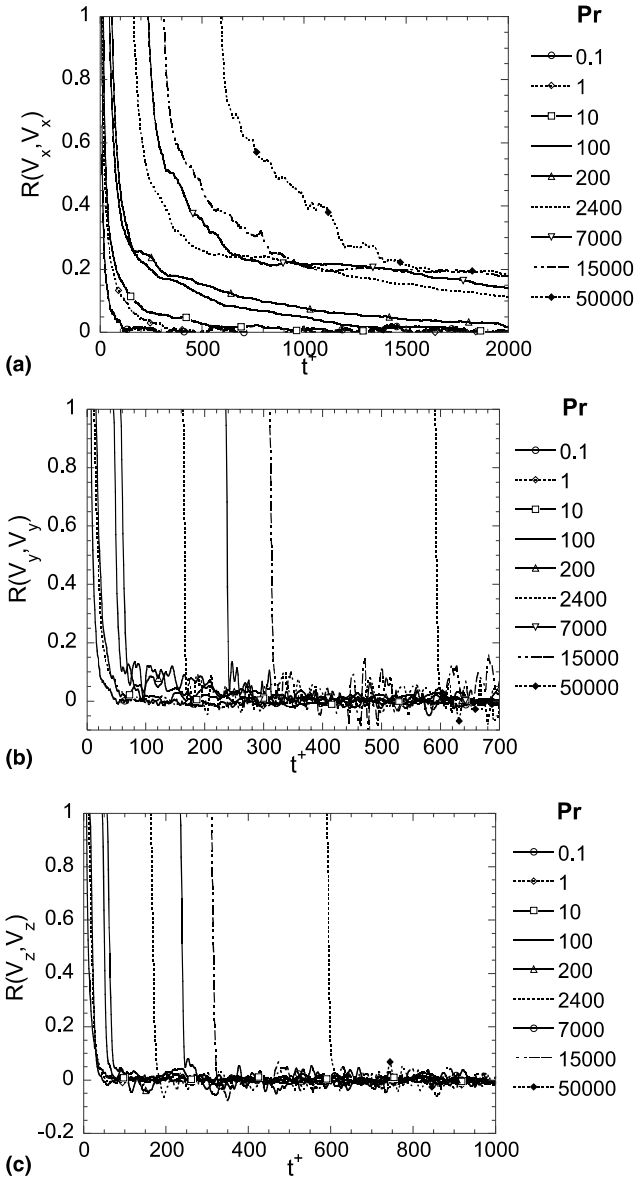

Fig. 11. Correlation coefficients for: (a) the streamwise; (b) the normal; (c) the spanwise marker velocities.

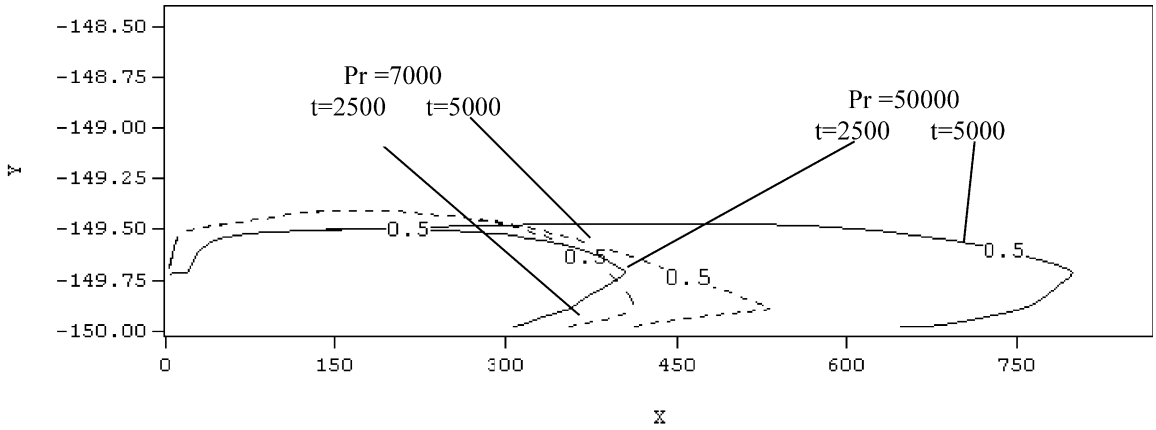

Fig. 12. Snapshots of a plume of high Pr markers at two different times from the initiation of particle release: $Pr = 7000$ (dashed lines) and $Pr = 50\,000$ (solid lines).

dominant transport mechanism. The time extent of this sub-regime can be quantified by a comparison of the rate of dispersion of the cloud in the normal direction, $\mathrm{d}\overline{Y^2}/\mathrm{d}t$, with the rate of dispersion predicted by Einstein's theory for molecular diffusion (Eq. 1). Fig. 9 presents the comparison between dispersion dominated by Brownian motion and the measured dispersion at the early stages of the cloud development. Fig. 10 shows the values of this timescale when zone I is defined to be 95% dominated by molecular diffusion, τ_{95}, as a function of Pr. Regression analysis shows that

$$\tau_{95} = 8.34Pr^{0.38}. \tag{8}$$

The second sub-regime of zone I, which is much longer than the first sub-regime, is identified as the stage at which transport is dominated by molecular effects; the molecular diffusion as well as the molecular viscosity of the fluid. The extent of this regime depends on the Pr of the fluid. Fig. 10 also presents the timescale that defines the end of zone I and the beginning of zone II as a function of Pr. This timescale is estimated using the points in Fig. 8(b) at which there is a change of the curve slope. It is found that

$$\tau_{\text{zone II}} = 27.1Pr^{0.36}. \tag{9}$$

The end of zone II and the beginning of zone III is marked in Fig. 8(b) and presented as a function of Pr in Fig. 10. The correlation for this transition is

$$\tau_{\text{zone III}} = 101.2Pr^{0.35}. \tag{10}$$

The marker velocity at the end of the dispersion sub-regime, τ_{95}, is used to calculate the marker velocity correlation functions presented in Fig. 11. The material correlation is calculated similar to the material correlation defined by Saffman (1960) as

$$R_{V_iV_j}(t,\tau_{95}) = \frac{\overline{V_i'(t-\tau_{95})V_j'(\tau_{95})}}{\left(\overline{V_i'^2(t-\tau_{95})}\right)^{1/2}\left(\overline{V_j'^2(\tau_{95})}\right)^{1/2}}. \tag{11}$$

The overbar denotes ensemble average over the total number of markers in the flow field and the prime denotes Lagrangian fluctuations, $V_i' = V_i(t) - \overline{V}_i(t)$. The streamwise–streamwise, $R_{V_xV_x}(t,\tau_{95})$, the normal–normal, $R_{V_yV_y}(t,\tau_{95})$, and the spanwise–spanwise, $R_{V_zV_z}(t,\tau_{95})$, correlations are shown in Figs. 11(a), (b), and (c), respectively. As Pr increases, the streamwise velocity correlation increases, which indicates that turbulence takes longer to start mixing the higher Pr cloud. On the contrary, the normal–normal and spanwise–spanwise correlations drop to zero very fast for all Pr fluids. The $R_{V_zV_z}(t,\tau_{95})$ figure shows that the correlation of the marker velocity in the spanwise direction does not appear to have a periodic increase. This is an indication that the markers do not align themselves with coherent, low or high-velocity streaks, which are known to exist close to the wall. However, this issue needs further investigation by studying the probability of a marker to be at a location in the flow field given that this location is part of a low or a high speed streak at the viscous wall region.

The behavior of a continuous source located at x_0 can be simulated by integrating the probability density function that describes the behavior of the puffs in time:

$$P_2(X - x_0, Y, t) = \int_{t_0}^{t} P_1(X - x_0, Y, t|t_0, \underline{x}_0)\,\mathrm{d}t. \tag{12}$$

Fig. 12 presents contours of this probability density function for $Pr = 7000$ and $Pr = 50\,000$. Even after 5000 viscous time units, the heat plume stays very close to the wall at high Pr. Integration of P_2 with x would provide the behavior of a heated plane.

5. Conclusions

The behavior of instantaneous line sources of heat or mass at the wall of a turbulent channel flow has been

investigated and has been characterized in this work. The effect of different *Pr* in turbulent transport has also been studied. The range of the fluid molecular *Pr* extends from 0.1 to 50 000. The use of LST allows qualitative observations as well as quantitative measurements in these cases. It provides a fundamental physical interpretation of Eulerian phenomena, such as the filtering effect of the wall to velocity frequencies that contribute to scalar transport, and the shape of the mean temperature profile for the case of a heated wall.

Three stages in the evolution of a puff were identified:

(i) The molecular diffusion dominated zone, which is further separated in two sub-regimes. The first sub-regime depends on the thermal diffusivity of the fluid and governs the initial development of the thermal cloud. The second sub-regime depends on both the diffusivity and the viscosity of the fluid and its extent is a function of *Pr*.
(ii) The transition zone, in which markers are leaking away from the original compact cloud of markers. This zone is logarithmic and it also depends on *Pr*.
(iii) The final zone, in which there are no *Pr* effects and the marker motion is dominated by turbulent convection.

In conclusion, understanding the behavior of individual heat sources can lead to the understanding of the macroscopic turbulent heat transport behavior. The challenge is to model and predict the behavior of such sources in time and space.

Acknowledgements

This work was partially supported by the National Computational Science Alliance under CTS990021N and utilized the NCSA HP/Convex Exemplar SPP-2000 and the NCSA SGI/CRAY Origin2000. Access to data from Tom Hanratty's laboratory at the University of Illinois is gratefully acknowledged. The author also acknowledges the support of the Research Council at the University of Oklahoma through the Junior Faculty Research award.

References

Batchelor, G.K., 1964. Diffusion from sources in a turbulent boundary layer. Arch. Mech. Stos. 3 (6), 661–670.

Calmet, I., Magnaudet, J., 1997. Large-eddy simulation of high-Schmidt number mass transfer in a turbulent channel flow. Phys. Fluids 9 (2), 438–454.

Campbell, J.A., Hanratty, T.J., 1983. Mechanism of turbulent mass transfer at a solid boundary. AIChE J. 29, 221.

Churchill, S.W., 1996. A critique of predictive and correlative models for turbulent flow and convection. Ind. Eng. Chem. Res. 35, 3122–3140.

Churchill, S.W., 1997. Critique of the classical algebraic analogies between heat, mass, and momentum transfer. Ind. Eng. Chem. Res. 36, 3866–3878.

Corrsin, S., 1953. Remarks on heat transfer: an account of some features of the phenomenon in fully turbulent regions. In: First Iowa Symposium on Thermodynamics, Iowa State University.

Corrsin, S., 1959. Progress report on some turbulent diffusion research. Adv. Geophys. 6, 161–164.

Eckelman, D.L., Hanratty, T.J., 1972. Interpretation of measured variations of the eddy conductivity. Int. J. Heat Mass Transfer 15, 2231–2239.

Einstein, A., 1905. Uber die von der molekular-kinetischen Theorie der Warme geforderte Bewegung von in ruhenden Flussigkeiten suspendierten Teilchen. Ann. Phys. 17, 549.

Fackrell, J.E., Robins, A.G., 1982. Concentration fluctuations and fluxes in plumes from point sources in a turbulent boundary layer. J. Fluid Mech. 117, 1–26.

Hanratty, T.J., 1956. Heat transfer through a homogeneous isotropic turbulent field. AIChE J. 2 (1), 42–45.

Hanratty, T.J., Vassiliadou, E., 1988. Turbulent transfer to a wall at large Schmidt numbers. In: M. Hirata, N. Kasagi (Eds.), Transport phenomena in turbulent flows. Theory, experiment and numerical simulation. Hemisphere, New York, pp. 255–274.

Incropera, F.P., Kerby, J.S., Moffat, D.F., Ramadhyani, S., 1986. Convection heat transfer from discrete heat sources in a rectangular channel. Int. J. Heat Mass Transfer 29 (7), 1051–1058.

Kasagi, N., Shikazono, N., 1995. Contribution of direct numerical simulation to understanding and modeling turbulent transport. Proc. R. Soc. London A 451, 257–292.

Kasagi, N., Tomita, Y., Kuroda, A., 1992. Direct numerical simulation of passive scalar field in a turbulent channel flow. Trans. ASME 114, 598.

Kawamura, H., Ohsaka, K., Abe, H., Yamamoto, K., 1998. DNS of turbulent heat transfer in channel flow with low to medium-high Prandtl number fluid. Int. J. Heat Fluid Flow 19, 482–491.

Kawamura, H., Abe, H., Matsuo, Y., 1999. DNS of turbulent heat transfer in channel flow with respect to Reynolds and Prandtl number effects. Int. J. Heat Fluid Flow 20 (3), 196–207.

Kim, J., Moin, P., 1989. Transport of passive scalars in a turbulent channel flow. In: J.C. Andre, J. Cousteix, F. Durst, B.E. Launder, F.W. Schmidt, Whitelaw, (Eds.), Turbulent Shear Flows, vol. 6. Springer, Berlin, pp. 85–96.

Kontomaris, K., Hanratty, T.J., McLaughlin, J.B., 1993. An algorithm for tracking fluid particles in a spectral simulation of turbulent channel flow. J. Comput. Phys. 103, 231–242.

Lyons, S.L., Hanratty, T.J., McLaughlin, J.B., 1991a. Direct numerical simulation of passive heat transfer in a turbulent channel flow. Int. J. Heat Mass Transfer 34 (4/5), 1149–1161.

Lyons, S.L., Hanratty, T.J., McLaughlin, J.B., 1991b. Large-scale computer simulation of fully developed turbulent channel flow with heat transfer. Numer. Meth. Fluids 13, 999–1028.

Moin, P., Mahesh, K., 1998. Direct numerical simulation: a tool in turbulence research. Ann. Rev. Fluid Mech. 30, 539–578.

Na, Y., Papavassiliou, D.V., Hanratty, T.J., 1999. Use of direct numerical simulation to study the effect of Prandtl number on temperature fields. Int. J. Heat Fluid Flow 20 (3), 187–195.

Na, Y., Hanratty, T.J., 2000. Limiting behavior of turbulent scalar transport close to a wall. Int. J. Heat Mass Transfer 43 (10), 1749–1758.

Papavassiliou, D.V., Hanratty, T.J., 1997. Transport of a passive scalar in a turbulent channel flow. Int. J. Heat Mass Transfer 40 (6), 1303–1311.

Papavassiliou, D.V., Hanratty, T.J., 1995. The use of Lagrangian methods to describe turbulent transport of heat from the wall. Ind. Eng. Chem. Res. 34, 3359–3367.

Ponoth, S.S., McLaughlin, J.B., 2000. Numerical simulation of mass transfer for bubbles in water. Chem. Eng. Sci. 55, 1237–1255.

Poreh, M., Cermak, J.E., 1964. Study of the diffusion from a line source in turbulent boundary layer. Int. J. Heat Mass Transfer 7, 1083–1095.

Raupach, M.R., Legg, B.J., 1983. Turbulent dispersion from an elevated line source: measurements of wind concentration moments and budgets. J. Fluid Mech. 136, 111–137.

Shlien, D.J., Corrsin, S., 1976. Dispersion measurements in a turbulent boundary layer. Int. J. Heat Mass Transfer 19, 285–295.

Saffman, P.G., 1960. On the effect of the molecular diffusivity in turbulent diffusion. J. Fluid Mech. 8, 273–283.

Taylor, G.I., 1921. Diffusion with continuous movements. Proc. London Math. Soc. 24A, 196–212.

Tiselj, I., Pogrebnyak, E., Changfeng, L., Mosyak, A., Hetsroni, G., 2001. Effect of wall boundary condition on scalar transfer in a fully developed turbulent flume. Phys. Fluids 13 (4), 1028–1039.